

Preliminary research of terminal shock motion in tandem configuration turbine-based combined cycle inlet

J. Liu and H. Yuan

liujunnever@nuaa.edu.cn

yuan_hch7@sina.com

Jiangsu Province Key Laboratory of Aerospace Power Systems
College of Energy and Power Engineering
Nanjing University of Aeronautics and Astronautics
Nanjing
People's Republic of China

Z. Hua

AVIC Shenyang Aircraft Design and Research Institute
Shenyang
People's Republic of China

W. Chen and N. Ge

Jiangsu Province Key Laboratory of Aerospace Power Systems
College of Energy and Power Engineering
Nanjing University of Aeronautics and Astronautics
Nanjing
People's Republic of China

ABSTRACT

The pressure oscillation and terminal shock motion in a two dimensional inlet, which was designed for tandem configuration turbine-based combined cycle propulsion systems was investigated experimentally and numerically, respectively. The inlet was characterised by a bleed cavity upstream the inlet throat, an S-shape rectangular-to-circular diffuser and flowpaths for a turbine and a ramjet engine. The terminal shock motion was calculated through a second-order unsteady Reynolds-averaged Navier-Stokes scheme. The pressure and the terminal shock were unsteady when the combined cycle inlet operated at different conditions. With the terminal shock located in the throat and at the shoulder of the third ramp of the TBCC inlet, the pressure oscillation was significant and the shock exhibited unsteady streamwise motion with an oscillatory pattern. The amplitude of shock oscillation at these two conditions was 6 mm and 12mm, respectively. When the shock was located downstream of the throat and upstream of the cowl lip, it oscillated in a small range. We defined this motion as the

“shake” of the shock. This unsteady behaviour of the shock was caused by flow separation in the combined cycle inlet diffuser.

Keywords: hypersonic vehicle; combined cycle propulsion systems; tandem configuration turbine-based combined cycle inlet; terminal shock oscillation; wind-tunnel experiment; unsteady numerical simulation

NOMENCLATURE

A_{exit}	cross-section area of the turbojet/ramjet flowpath
$A_{\text{th,plug}}$	throat area near the plug
D_e	diameter of the diffuser exit plane
H_c	captured height of the inlet
H_{bleed}	height of the bleed cavity
H_t	height of the throat
L	length of the inlet model
L_d	length of the diffuser
f	frequency of pressure oscillation
M	flow or flight Mach number
P	static pressure
P_{∞}	free stream static pressure
P_{av}	average pressure
S_p	standard deviation of static pressure
PSD	power spectral density
T	non-dimensional time
TR	throttle ratio of turbojet/ramjet flowpath
δ_i	angle of compression ramp
σ	total pressure recovery
π	static pressure ratio

1.0 INTRODUCTION

Turbine-Based Combined Cycle (TBCC) propulsion systems have been extensively studied in recent years⁽¹⁻⁴⁾. It is one of the candidate propulsion systems for access to space. TBCC propulsion systems are reusable and enable horizontal take-offs that may significantly reduce launch costs and improve safety⁽⁵⁾. Turbine and ramjet engines are integrated into the propulsion system to enable future vehicles that operate across a broad range of Mach numbers, including the subsonic, supersonic and hypersonic flight regimes. The TBCC inlet is an essential component of the propulsion system. It is used to diffuse air from freestream velocity to a lower velocity acceptable for combined cycle systems in a broad range of Mach numbers⁽⁶⁾. Any unstable operation in a TBCC inlet may result in structural damage, engine surge or non-recoverable thrust loss⁽⁷⁾.

A number of experimental and numerical studies have performed on TBCC inlets, but few of them investigated shock oscillation. In the 1990s, the Japanese have implemented the Hypersonic Transport Propulsion System Research Project (HYPR). A sub-scale model engine of a ramjet for hypersonic transport was designed and tested in a freestream of Mach

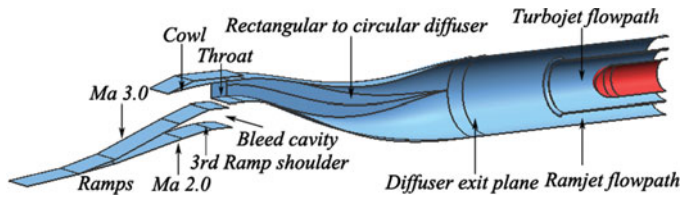


Figure 1. (Colour online) Tandem configuration TBCC inlet model.

5 in a ramjet engine test facility. The results indicate that the increase of the fluctuation of the shock position and pressure in the inlet lead to a decrease in the margin to unstart. Also, it was shown that the terminal shock position in the supersonic inlet can be controlled with fuel flow rate⁽⁸⁾. An experimental study was conducted to evaluate the performance of a TBCC inlet concept, consisting of a low speed turbojet inlet and high-speed dual-mode scramjet inlet at the NASA Langley Research Center. Results indicated that the inlets did not interact with each other sufficiently to affect inlet operability. Flow spillage resulting from a high-speed inlet unstart did not propagate far enough upstream to affect the low-speed inlet. Also, a low speed inlet unstart did not cause the high-speed inlet to unstart⁽⁹⁾. Zhang et al⁽¹⁰⁾ designed an over-/under-configuration TBCC inlet with a variable geometry bleed cavity. Numerical simulations and high-speed wind-tunnel experiments were conducted on this inlet to validate the feasibility of the scheme and the aerodynamic characteristics during TBCC inlet mode transition⁽¹¹⁾.

A great amount of experimental and numerical studies of shock oscillation have been done in regular supersonic and hypersonic inlets. For instance, the unstart oscillatory flow of mix-compression hypersonic inlet was investigated numerically by Fan et al⁽¹²⁾. The results showed that the dominant frequency of unstart oscillatory flow of hypersonic inlets is reduced by the bleeding of the boundary layer. A shock oscillation phenomenon in supersonic inlets was studied both numerically and experimentally by Nakayama et al⁽¹³⁾. The computed frequency and amplitude showed good agreement with those of the experiment. Ogawa et al⁽¹⁴⁾ investigated the shock wave oscillations occurring in the internal flow passage. The peak frequencies of the shock oscillation varied with the boundary-layer conditions.

In summary, the research of shock oscillation phenomena was performed for regular supersonic and hypersonic inlets. The investigation of TBCC inlets focuses on the design of the flowpaths and the inlet mode transition. The shock oscillation phenomenon in TBCC inlets has not been investigated yet. This paper investigates the shock oscillation phenomenon appearing at three different operating conditions of a tandem configuration TBCC inlet at Mach 2.0, both numerically and experimentally.

2.0 METHODOLOGY

2.1 Experiment

The tandem configuration TBCC inlet is designed to work within Mach 0-3.0 with mode transition at Mach 2.0. This paper investigates the shock oscillations at the mode transition point, which is critical for combined cycle propulsion systems. A model of the tandem configuration TBCC inlet at Mach number 2.0 and Mach number 3.0 is shown in Fig. 1. The TBCC inlet consists of three parts: supersonic external compression ramps, subsonic diffuser with rectangular section at the entrance transitioning to circular section at the exit,

Table 1
Main parameters of tandem configuration TBCC inlet

M	$\delta_1/^\circ$	$\delta_2/^\circ$	$\delta_3/^\circ$	H_c/mm	$H_{\text{bleed}}/\text{mm}$	H_t/mm	D_e/mm	L/mm	L_d/mm
2.0	6	2	4	100.0	31.7	30.0	110.0	1060.0	429.5

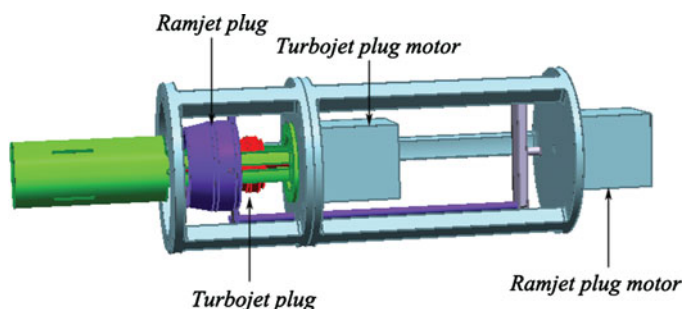


Figure 2. (Colour online) Tandem configuration TBCC inlet mass-flow plugs.

and turbojet/ramjet flowpaths. The compressed air flow is separated into two streams after the third ramp, one is bled out of the inlet through a bleed cavity and the other enters the diffuser. The function of the bleed cavity is to bleed the mass flow at off-design condition. Boundary-layer bleed may also help prevent inlet unstart at the mode transition point. The diffuser geometry was designed mathematically according to Ref.15. After the diffuser, the passage is separated into two passages; the inner circular passage is the turbojet flowpath and the outer annular passage is the ramjet flowpath. The area ratio of the turbojet flowpath to the ramjet flowpath is 0.77. The main parameters of the inlet are listed in Table 1. Among them, $\delta_1 \sim \delta_3$ are three angles of external compression ramps, H_c is the captured height of the inlet, H_{bleed} is the height of bleed cavity, H_t is the height of the throat, D_e is the diameter of the diffuser exit plane, L is the length of the inlet model and L_d is length of the diffuser.

The operational modes of engines can be simulated by turbojet and ramjet mass-flow plugs. These two plugs are placed at the exit of the two flowpaths (Fig. 2). The positions of the two plugs are controlled by two motors, so the movement of the turbojet and ramjet plugs can be controlled separately. The Throttling Ratio (TR) is used to define the axial positions of these two plugs according to

$$TR = (1 - A_{th, \text{plug}}/A_{\text{exit}}) \times 100\%, \quad \dots (1)$$

where $A_{th, \text{plug}}$ is the throat area near the plug and A_{exit} is the cross-sectional area of the turbojet/ramjet flowpath. During a wind-tunnel experiment, TR can be set to any value between 0% (fully opened) and 100% (fully closed).

The experiment was conducted at the NH-1 high-speed wind tunnel of Nanjing University of Aeronautics and Astronautics. The facility runs in a blow-down mode with a usable run time greater than 40 s. The tunnel has a rectangular working section with a constant cross-section 600 mm wide by 600 mm high, and the length of the working section is 1,580 mm. In the experiment, the inflow Mach number is 2.0, the total temperature is 300K, the total pressure is 208 kPa and the turbulence of the inflow is about 0.3%-0.45%. During the test,

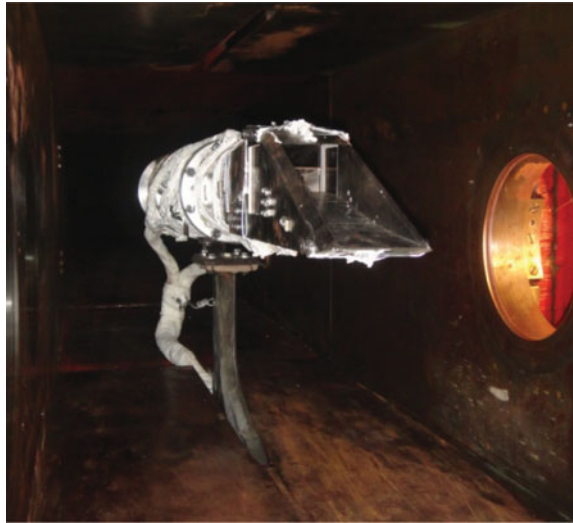


Figure 3. (Colour online) Tandem configuration TBCC inlet model in NH-1 high-speed wind tunnel.

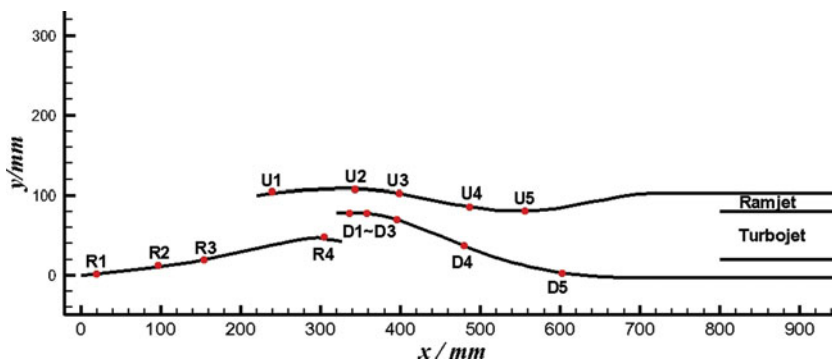


Figure 4. (Colour online) High-response pressure transducers in TBCC inlet.

the angles of attack and yaw were 0° , and only the throttle ratio of the turbojet and ramjet flowpaths changed.

Low- and high-response static pressure measurements were performed by two systems. Low-response pressure measurements were performed by a PSI9001 series pressure scanner system at 30 samples per second with the range of 500 kPa and accuracy of $\pm 0.05\%$ F.S. High-response pressure measurements were performed by dynamic pressure transducers and a TST5913 data acquisition system at 10,000 samples per second. The transducers are labelled by R1–R4, D1–D5 and U1–U5 in Fig. 4. These transducers have an accuracy of $\pm 0.2\%$ F.S. of the full range (500 kPa) and a natural response frequency of 50 kHz.

2.2 Numerical simulation

Numerical simulations of the steady and unsteady flow fields were performed with the FLUENT solver. The unsteady Reynolds-averaged Navier-Stokes equations in three dimensions are solved by using a finite volume spatial discretisation method. In the

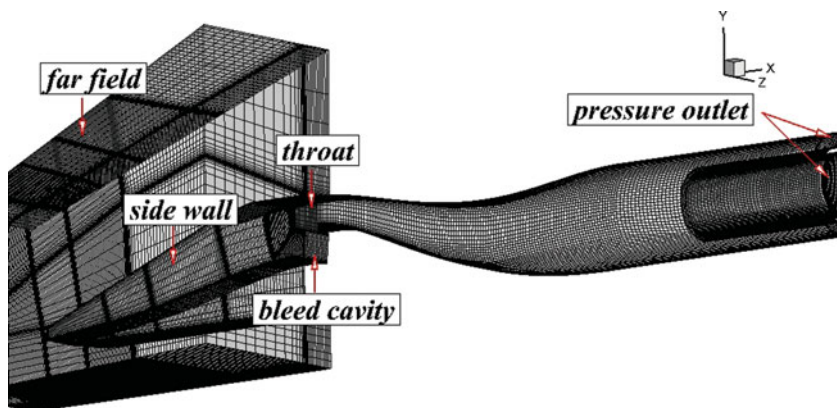


Figure 5. (Colour online) Typical computational mesh used for steady and unsteady calculations (600,000 cells).

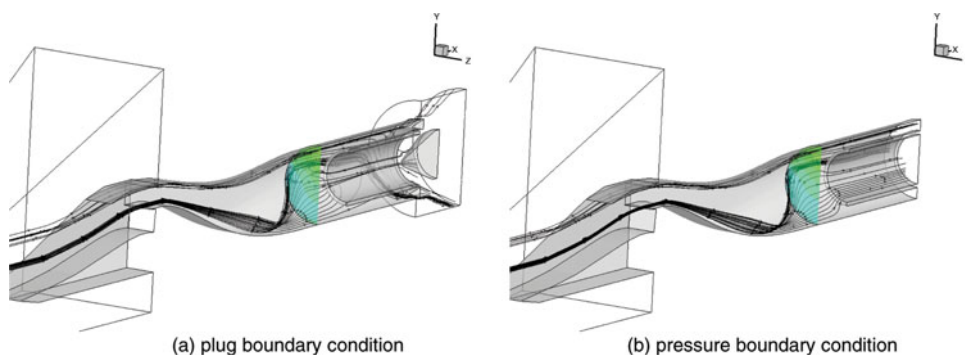


Figure 6. (Colour online) Flow visualisation of TBCC inlet with different boundary conditions.

computations, the inviscid flux scheme is Roe's method and the monotonic upwind scheme for conservation laws (MUSCL) approach is used for variable extrapolation⁽¹⁶⁾. The turbulent flow is modelled by the Spalart-Allmaras⁽¹⁷⁾, of which the governing equations are discretised by a second-order upwind scheme. The wall function was used in the near wall region in this research. The fluid is treated as compressible ideal gas. The computational domain includes the flow field surrounding the tandem TBCC inlet and its boundary condition is set as pressure far-field. The no-slip adiabatic wall conditions are imposed in the solid wall boundaries. The geometry is symmetrical and the yaw angle of the model is equal to 0°. The flowfield is symmetrical, too. Therefore, the computational domain is chosen just as the half of the actual one and the symmetry boundary condition was used. Dual-time stepping method is used in the unsteady simulation. A typical computational mesh is shown in Fig. 5.

In the experiment, turbojet and ramjet plugs are used to simulate the operating modes of both engines. In the computational fluid dynamics (CFD) simulation, two different boundary conditions were compared. One is the plug boundary condition, which uses a plug to simulate the operating modes of engines. The other is a pressure outlet boundary condition, which uses pressure to simulate the operating modes of engines. Figures 6 and 7 show streamlines and total pressure contour of two different sections at different boundary conditions. From these

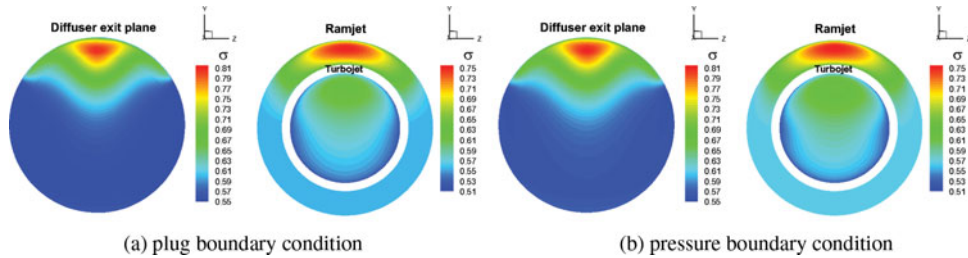


Figure 7. (Colour online) Total pressure of TBCC inlet with different boundary conditions.

two figures, we can note that the difference between the two boundary conditions is small. In addition, the pressure boundary condition is more flexible than the plug boundary condition. It is easy to change the backpressure of the turbojet/ramjet flowpaths when the operational condition of the turbojet/ramjet engines change. But for the plug boundary condition, it is more complicated. The axial positions of the two mass flow plugs should change; thus, the model should be re-meshed. The pressure boundary condition was adopted in the present work.

3.0 RESULTS

As we know, the inlet is used to compress the airflow through the external compression ramps, internal contraction and the diffuser. In the supersonic inflow, the oblique shock generates from ramps; after the oblique shock, the static pressure increases slightly. Then the airflow is compressed through the contraction of the flowpath. The throat, which is the minimum cross-sectional area in the inlet system, comes after this contraction of the flowpath. Ideally, a terminal shock, which increases the static pressure of the airflow significantly and decreases the airflow from supersonic to subsonic non-linearly, is designed to be located at the throat. Finally, the pressure of the airflow increases steadily through the diffuser. During the wind-tunnel test, the oblique shock and terminal shock can be characterised through the static pressure along the flowpath.

The wind-tunnel experiment was conducted at the condition of keeping the ramjet flowpath throttle ratio constant and increasing the turbojet flowpath throttle ratio steadily. Figure 8 shows the wall static pressure measured by low-response pressure transducers along the flowpath at the condition of $TR_{\text{ramjet}} = 80\%$ and different TR_{turbojet} . The six turbojet throttle ratios are 15.0%, 26.0%, 32.6%, 40.0%, 48.1% and 57.0%, respectively. At each throttle ratio, the turbojet plug was fixed for 4–5 s for data acquisition. From Fig. 8, we found that in the first TR, the terminal shock was located downstream of the throat; in the second TR, the terminal shock was located at the throat. In the first two TRs, the operating condition of the TBCC inlet was supercritical. In the third TR, the terminal shock was located at the shoulder of the third ramp. The operating condition of the TBCC inlet was critical. In the last three TRs, the terminal shock was located upstream the cowl lip, and the TBCC inlet operated at a subcritical condition.

Figure 9 shows the wall static pressure measured by high-response transducers as the throttle ratio of the turbojet flowpath increased. There are six TRs of wall static pressure signal during a test. Wall static pressure oscillated at each TR with different amplitudes. From the difference between D3 and D2 pressure signals in the first TR of the test, we infer that

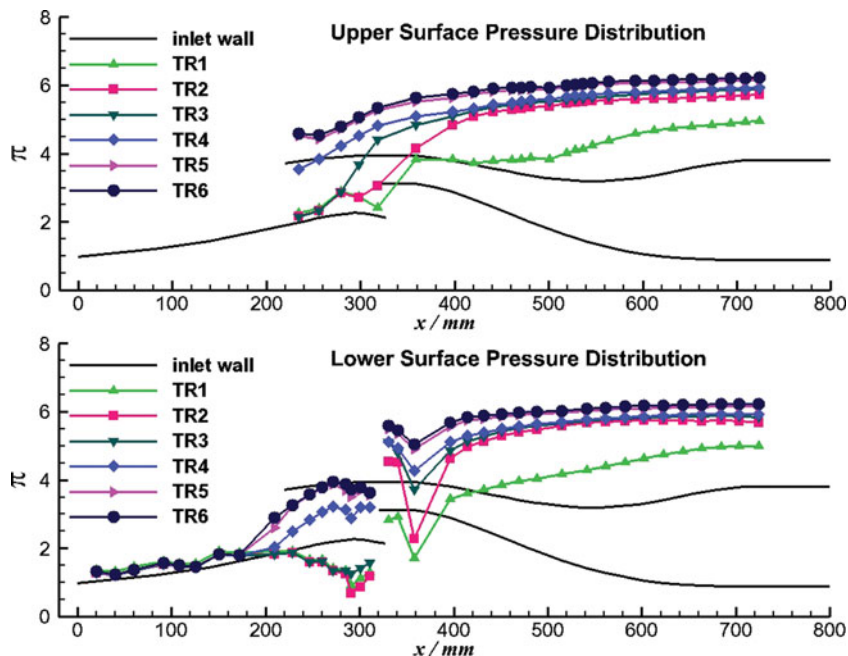


Figure 8. (Colour online) Low-response wall static pressure along the flowpath at different TRs.

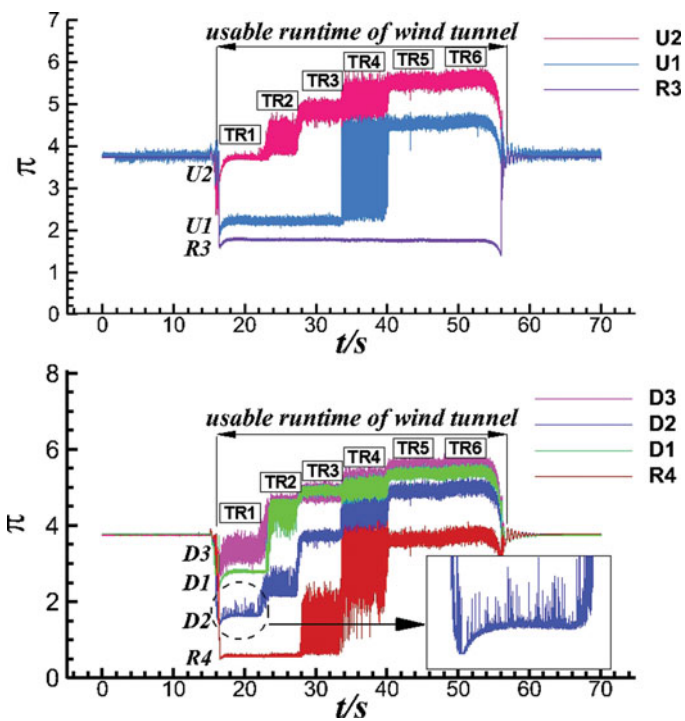


Figure 9. (Colour online) High-response wall static pressure at different TRs.

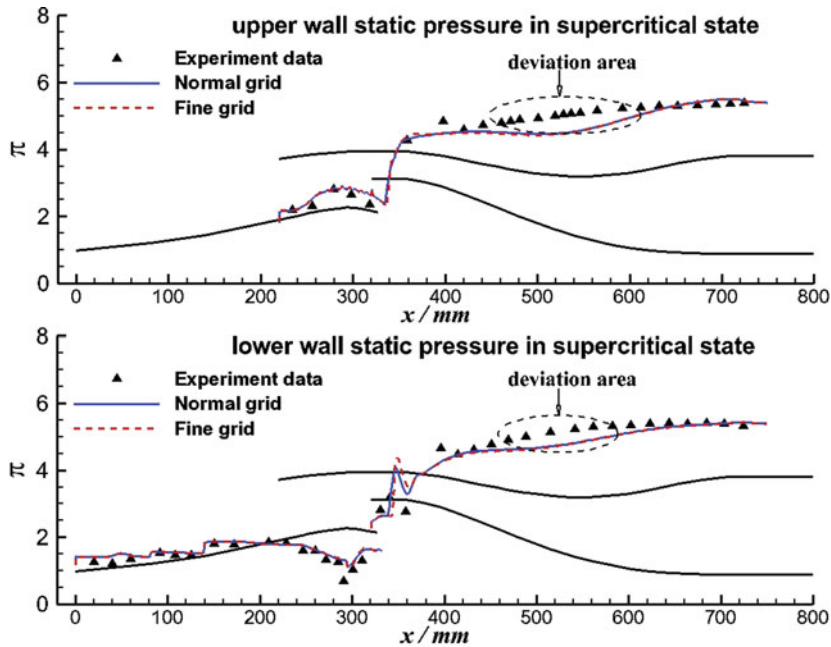


Figure 10. (Colour online) The wall static pressure distribution with the terminal shock located in the diffuser.

the terminal shock was located between the D2 and D3 pressure transducers. The enlarged zone in Fig. 9 indicated that the terminal shock is unstable. In the second TR, the pressure at the D1 probe increases rapidly, so the terminal shock is located in front of the D1 probe. The pressure fluctuations measured at the D1, D2 and U2 probes may be caused by the oscillation of the terminal shock. In the third TR, the pressure at the R4 probe oscillated dramatically indicating that the terminal shock moved forward to the shoulder of the third ramp and remained unstable. In the fourth TR, the pressure at the U1 probe oscillated even more than at the R4 probe. That indicated the terminal shock was extremely unstable near the U1 probe. In the last two TRs, the pressure fluctuations were not as dramatic as before. The pressure signal at the R3 probe almost remained steady in the test, which means the terminal shock remained behind the R3 probe, even with the terminal shock located upstream of the cowl.

The results of the experiment indicate that the terminal shock was unstable in the diffuser, at the shoulder of the third ramp and upstream the cowl lip. Unsteady numerical simulation was conducted, based on the inflow conditions of the wind-tunnel experiment, to analyse the terminal shock motion in the tandem configuration TBCC inlet, as the operating condition of the engines was varied.

3.1 Terminal shock located in the diffuser

Figure 10 shows the comparison between numerical simulation results and experimental data with the terminal shock located in the diffuser. The numerical simulation results fit well with experimental data, except for some deviation in the second bend of the diffuser. The difference was caused by the over-prediction of the separation bubble. The flowpath is narrowed by

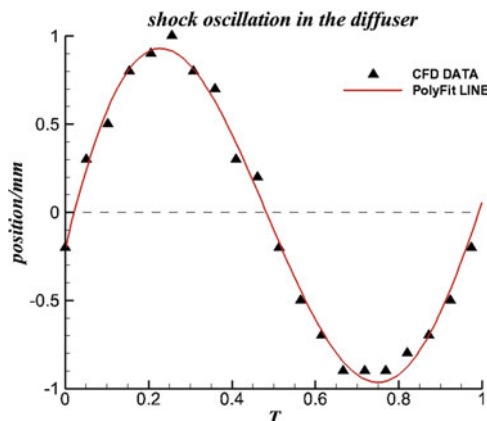


Figure 11. (Colour online) The terminal shock oscillation in the diffuser.

the bubble and the flow is accelerated. That makes the pressure in CFD smaller than the experimental data. The results of the normal grid (600,000 cells) were consistent with the fine grid (1,230,000 cells). The difference of the parameters in the diffuser exit plane is smaller than 0.1% in these two cases. The numerical simulation method was found to be adopted to investigate the flowfields in a tandem configuration TBCC inlet.

The total time of unsteady simulation is 16 ms. The characteristics of the D3 probe pressure signal is oscillatory, and within the total time, there are four periods of oscillation. The terminal shock motion in a period when it was located in the diffuser is presented in Fig. 11. The points are the numerical results at each time step, the curve is the PolyFit result of the CFD data. The character of terminal shock motion is similar to a sine curve. The zero position of the terminal shock oscillation is $x = 354.4$ mm, and the amplitude of the shock oscillation is 1 mm.

The standard deviation of static pressure in a period of time, which indicates the amplitude of the pressure fluctuation is defined in Equation (2) as

$$S_p = \sqrt{\frac{1}{n} \sum_{i=1}^n (P_i - P_{av})^2}, \quad \dots (2)$$

where P_{av} is the average pressure at a specific TR, and n is the number of data points used. The standard deviation of the inflow static pressure is 0.50 kPa, however, at the D3 probe, it increases up to 3.65 kPa. The power spectral density of the static pressure signal indicates the main frequency of pressure fluctuation. As Fig. 12 shows, the frequency of the pressure fluctuation in the experimental data varies from 141 Hz to 214 Hz, and in the CFD, it is between 200 Hz and 350 Hz. The pressure fluctuation is inferred to be caused by flow separation. The numerical simulation over-predicted the flow separation and caused the difference in frequency distribution between the experiment and CFD.

After reconsideration, we defined the unsteady phenomenon in the first TR as the “shake” of terminal shock rather than oscillation, because the amplitude of shock motion in the first TR was only 3.33% of the height of the inlet throat. The main cause of the unsteadiness of terminal shock would be the separation bubble on the diffuser sidewall (Fig. 13). The boundary layer

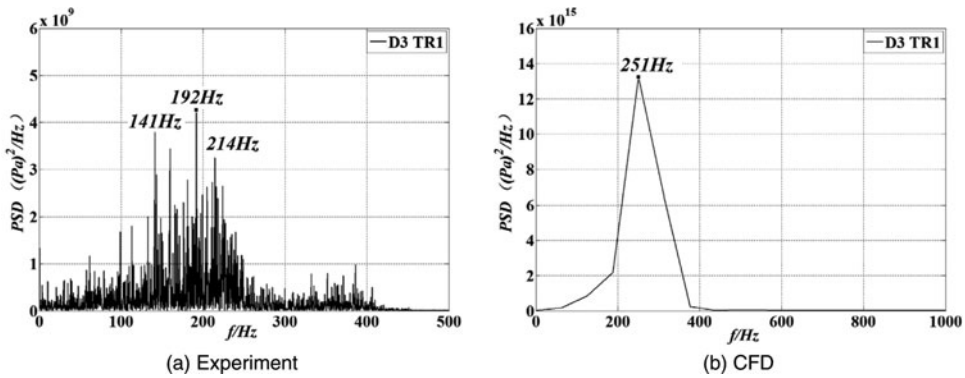


Figure 12. (Colour online) The terminal shock oscillation frequency as the shock in diffuser.

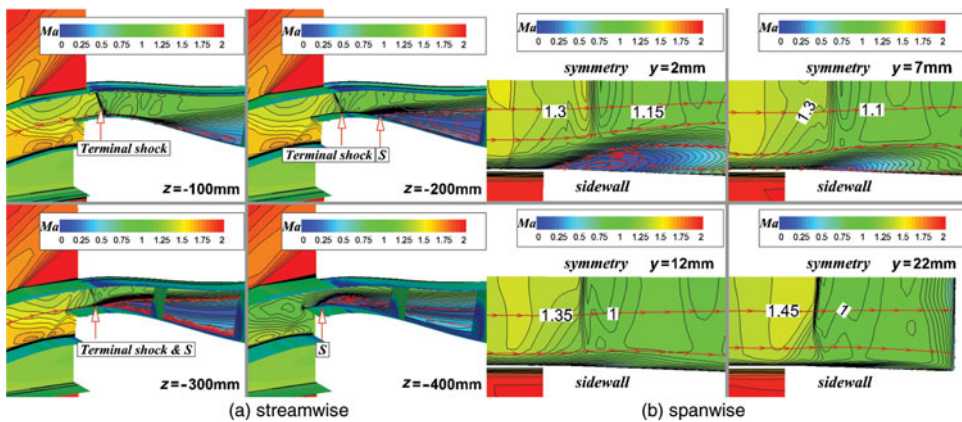


Figure 13. (Colour online) Streamwise and spanwise slices of Mach number contours as the shock in diffuser.

on the sidewall within the diffuser develops, starting from the sidewall of the inlet, making it easier to separate. The terminal Shock/Boundary-Layer Interactions (SBLIs) cause the separation to occur on the diffuser sidewall. Figure 13(a) shows a streamwise slice of Mach number between the slice and the symmetry plane at a distance of 100 mm, 200 mm, 300 mm and 400 mm, respectively; as the figure shows, when the distance between the slice and the symmetry plane increases, the separation bubble develops. At $z = -300$ mm, the start point of the separation bubble was located right behind the terminal shock. At $z = -400$ mm, which is close to the sidewall, the terminal shock disappears and a big separation bubble shows up. The separated flow contains a point of inflection in the velocity profile. Such profiles are known to be unstable (Rayleigh's first theorem), and spatial stability theory has been used to show that the separated region will amplify disturbances over a narrow frequency range⁽¹⁸⁾. This unstable nature of the separation bubble is the source of the unstable behaviour of the terminal shock and the fluctuation of pressure. Figure 13(b) shows the spanwise slice of Mach number, and the distance between each slice and lower wall are 2 mm, 7 mm, 12 mm, and 22 mm, respectively. Detailed flow fields of the SBLIs are shown in the $y = 2$ mm. The separation bubble on the side wall narrows the passage. At the same time, the streamlines are curved and turn towards the symmetry plane at the separation bubble. As the value of y increases,

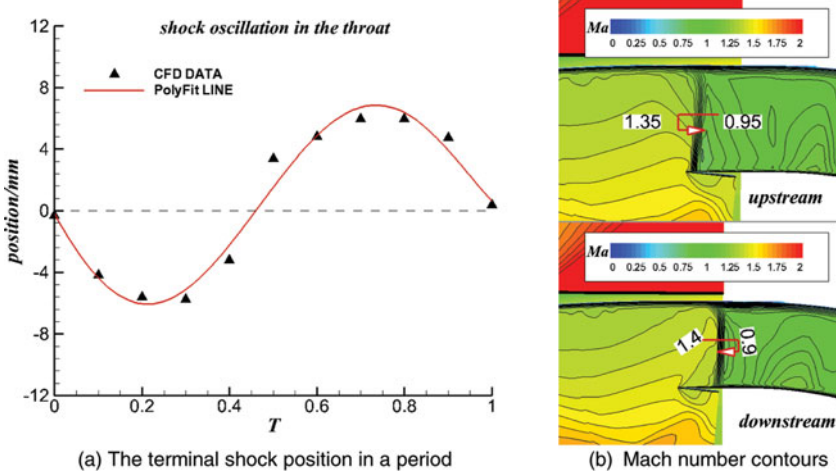


Figure 14. (Colour online) Terminal shock oscillation amplitude and Mach number contours as shock in the throat.

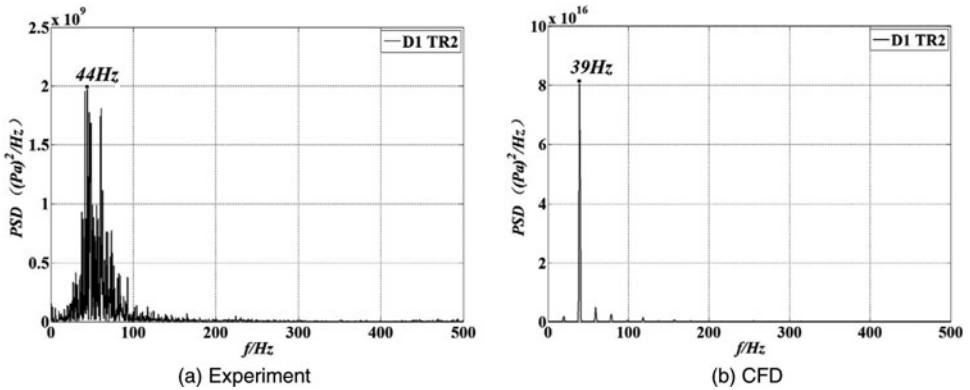


Figure 15. Terminal shock oscillation frequency as shock in the throat.

the separation disappears gradually and the streamlines stay parallel with the sidewall. At $y = 22$ mm, the terminal shock became λ shock in the spanwise direction.

In the second TR, the terminal shock moved from the diffuser to the throat. The amplitude of shock oscillation increased up to 6mm (Fig. 14(a)); the zero position of shock oscillation was $x = 329.5$ mm of the inlet model. Figure 14(b) shows the most upstream and downstream position of the terminal shock during the oscillation. As the figure illustrates, the Mach number before the terminal shock is about 1.4. During the shock oscillation period, the shock was always in the inlet throat. The standard deviation of static pressure measured at the D1 probe is 4.10 kPa, and the main pressure fluctuation frequency was about 44 Hz (Fig. 15(a)). However, the oscillation frequency in the CFD was 39 Hz (Fig. 15(b)). The numerical simulation was quite close to the experimental data.

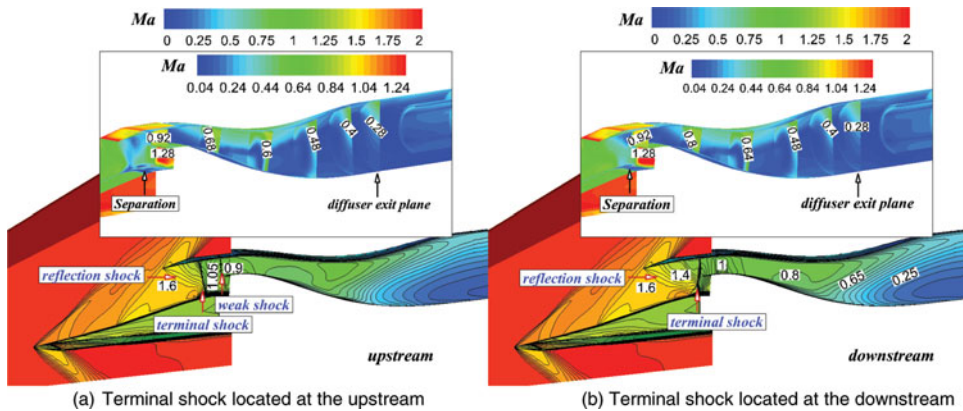


Figure 16. (Colour online) Mach number contours of TBCC inlet as the shock in the third ramp shoulder.

3.2 Terminal shock located at the shoulder of the third ramp

In the third TR, the terminal shock moved from the throat to the third ramp of the TBCC inlet. The operating condition of the TBCC inlet transitioned from supercritical to critical. In general, this type of inlet can't operate at the critical condition. However, the TBCC inlet investigated in the present work can operate at this condition because of the bleed cavity behind the third ramp. Figure 16 shows the most upstream and downstream position of the terminal shock during the oscillation in third TR. As the figure shows, when the terminal shocks are located at the upstream position, the separation bubble is at the shoulder of the third ramp and a weak shock stays at the entrance of the diffuser. When the terminal shock is at the downstream position, the terminal shock becomes a λ shock. The separation bubble in the diffuser develops gradually. The separation occurring in the diffuser and at the shoulder could be the main reason for the mutability of the terminal shock.

Figure 17 shows the terminal shock oscillation amplitude and frequency in the third TR. The amplitude of the oscillation was about 12 mm. The main frequency of the R4 pressure signal obtained in the experiment was about 56–67 Hz, while CFD predicted a frequency of 89 Hz. The difference may be caused by the deviation of the back pressure at the bleed cavity. When the shock was located at the shoulder of the third ramp, it was affected by the back pressure of the diffuser exit plane and the bleed cavity. The standard deviation of static pressure measured at the R4 probe is 12.87 kPa, which was greater than the shock instability in the diffuser.

3.3 Terminal shock located upstream of the cowl

In the fifth TR, the terminal shock moved from the shoulder of the third ramp to the upstream of the TBCC inlet cowl lip, and the operating condition of the TBCC inlet transitioned from critical to subcritical. In general, inlet buzz would occur with its characteristic large amplitude pressure fluctuations and travelling shock waves^(19–22). However, in the fifth TR, the standard deviation of pressure at the U1 probe, which was located right behind the terminal shock, was only 1.40 kPa. It was even smaller than the amplitude of oscillation with the shock located within the diffuser. That indicates the pressure fluctuations were small when the TBCC inlet operated at the subcritical condition. Figure 18 shows the Mach number contour in the fifth TR. As the figure illustrates, when the terminal shocks were located upstream the cowl lip, the

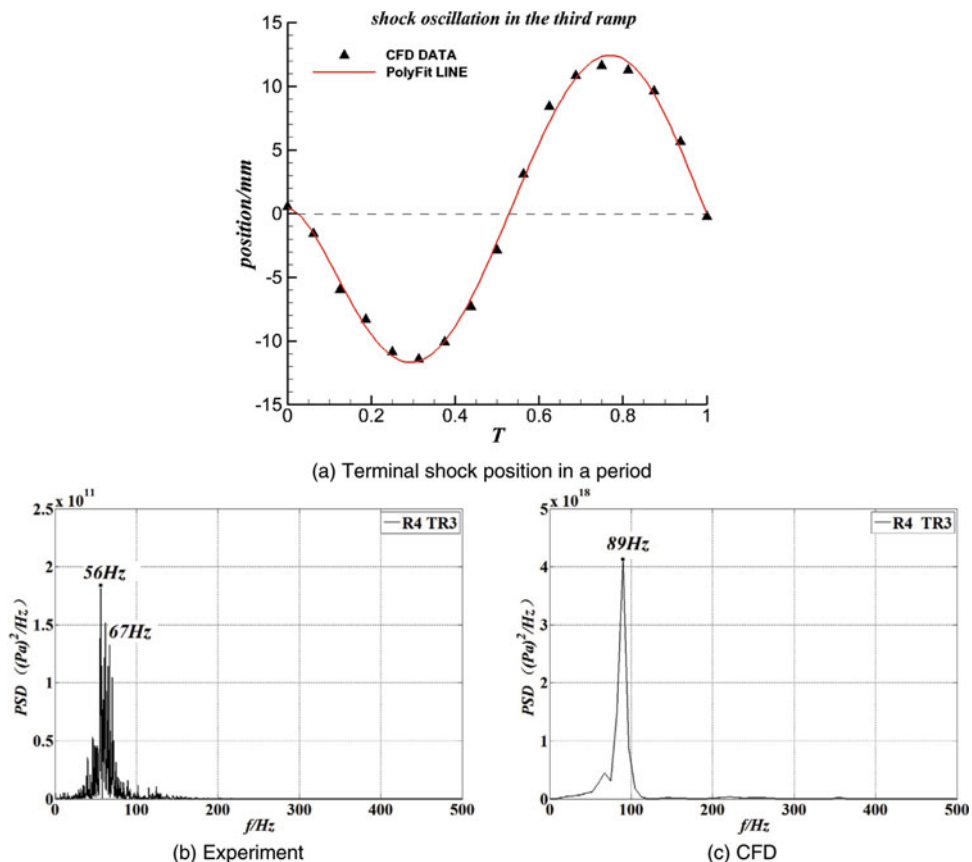


Figure 17. (Colour online) Terminal shock oscillation amplitude and frequency as the shock in the third ramp shoulder.

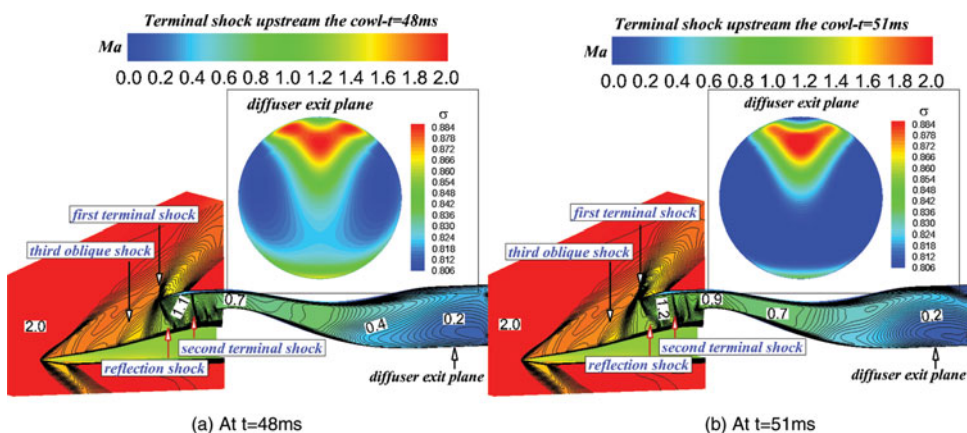


Figure 18. (Colour online) Mach number and total pressure contours of TBCC inlet as the shock upstream the cowl.

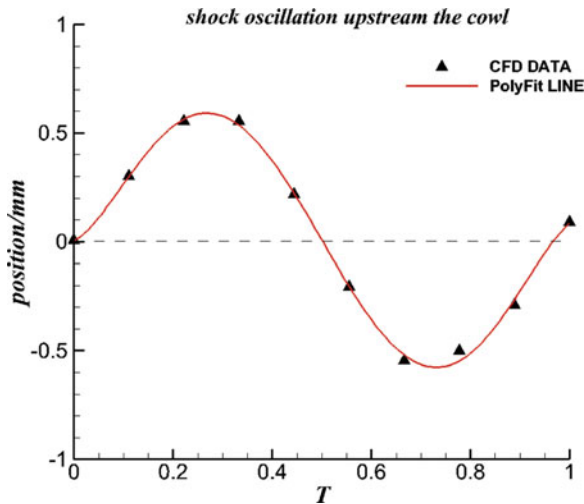


Figure 19. (Colour online) Terminal shock oscillation amplitude as the shock upstream the cowl.

third oblique shock merged with the first terminal shock. There were two terminal shocks in the inlet; the first terminal shock was an oblique shock located upstream the cowl lip, and the second terminal shock was a normal shock at the shoulder of the third ramp. Between the two terminal shocks, there was a reflection shock generated from the cowl lip. The angle of this reflection shock was obviously greater than the third TR (Fig. 16), because the Mach number in front of the reflection shock was smaller than in the preview case. From Fig. 18, we see that the position of the first terminal shock did not change appreciably. However, the total pressure in the diffuser exit plane did change significantly. This suggests the flow in the diffuser is fully unsteady.

The unsteady flow in the diffuser causes the unsteady motion of the terminal shock. After detailed analysis of shock position, the character of shock motion in a period is shown in Fig. 19. The amplitude of the first terminal shock oscillation was 0.6 mm, only 2% of the height of the throat. It was even smaller than the amplitude of shock motion in the first TR. We, therefore, define the shock motion in the fifth TR as the “shake” of the shock, which was the same as the first TR.

4.0 CONCLUSIONS

The present work focuses on the investigation of pressure oscillation and terminal shock motion in a two-dimensional inlet designed for tandem configuration Turbine-Based Combined Cycle (TBCC) propulsion systems. The tandem configuration TBCC inlet is a mixed compression inlet consisting of three ramps, an S-shaped rectangular to circular diffuser, and flow paths of both a turbine and a ramjet engine. The characteristic of low- and high-response pressure which is measured in the high-speed wind-tunnel test along the flowpath was analysed and a three-dimensional unsteady numerical study of terminal shock motion with the shock located at three different positions within the inlet, including entrance of the diffuser, the shoulder of the third ramp and upstream of the cowl lip at Mach 2.0, were investigated.

High-speed wind-tunnel experiment results indicate that when the operating condition of the combined cycle propulsion systems changed, the position of the terminal shock changed gradually. At the same time, at each position, the terminal shock motion was different. When the terminal shock was located downstream of the throat and upstream of the cowl lip, the standard deviation of the pressure signal was 3.65 kPa and 1.40 kPa, respectively. When terminal shock moved upstream to the throat, the frequency measured by the D1 probe was about 44 Hz, and the standard deviation at the D1 probe was 4.10 kPa. As the terminal shock moved forward to the shoulder of the third ramp, the frequency at the R4 probe was about 56 Hz, and the standard deviation at the R4 probe was 12.87 kPa.

The computations were performed using a second-order unsteady Reynolds-averaged Navier-Stokes scheme. The results indicate that when the terminal shock is located downstream of the throat and upstream of the cowl lip, the amplitude of shock motion is small, defined as the “shake” of the terminal shock. When the shock is located in the throat and at the shoulder of the third ramp, significant shock oscillation occurs, and the shock oscillation frequency is about 20 Hz and 45 Hz, and the amplitude is about 6 mm and 12 mm, respectively.

ACKNOWLEDGEMENTS

The present research was funded under the Fundamental Research Funds for the Central Universities (No. NS2015025), Funding for Outstanding Doctoral Dissertation in NUAA (No. BCXJ16-01) supported by the Fundamental Research Funds for the Central Universities and Aviation Foundation Project (No. 2015ZB52016).

REFERENCES

1. HIRAIWA, T., ITO, K., SATO, S. et al. Recent progress in scramjet/combined cycle engines at JAXA, Kakuda space center. *Acta Astronautica*, April 2008, **6**, (3), pp 565-574. doi: [10.1016/j.actaastro.2008.04.011](https://doi.org/10.1016/j.actaastro.2008.04.011).
2. WALKER, S., TANG, M. and MAMPLATA, C. TBCC propulsion for a Mach 6 hypersonic airplane, AIAA Paper 2009-7238, 2009.
3. FERNÁNDEZ-VILLACÉ, V., PANIAGUA, G. and STEELANT, J. Installed performance evaluation of an air turbo-rocket expander engine. *Aerospace Science and Technology*, May 2014, **35**, pp 63-79. <http://dx.doi.org/10.1016/j.ast.2014.03.005>.
4. WANG, Z.G., WANG, Y., ZHANG, J.Q. et al. Overview of the key technologies of combined cycle engine precooling systems and the advanced applications of micro-channel heat transfer. *Aerospace Science and Technology*, August 2014, **3**, (9), pp 31-39. <http://dx.doi.org/10.1016/j.ast.2014.08.008>.
5. BILARDO, V.J., CURRAN, F.M., HUNT, J.L. et al. The benefits of hypersonic airbreathing launch systems for access to space, AIAA Paper 2003-5265, 2003.
6. MAHONEY, J.J. Inlets for supersonic missiles, AIAA Education Series, 1990.
7. MARSHALL, A.W., GUPTA, A.K. and LEWIS, M.J. Critical issues in TBCC modeling, AIAA Paper 2004-3827, 2004.
8. TAKAO, O., YOSHINARI, E., HIDEMASA, N. et al. Experimental approach to the HYPR Mach 5 ramjet propulsion system, AIAA Paper 1998-3277, 1998.
9. ALBERTSON, C.W., EMAMI, S. and TREXLER, C.A. Mach 4 test results of a dual-flowpath, turbine based combined cycle inlet, AIAA Paper 2006-8138, 2006.
10. ZHANG, H.J., GUO, R.W. and XIE, L.R. Study of variable geometry bleed cavity of TBCC inlet, *J Aerospace Power*, December 2012, **27**, (12), pp 2714-2723. doi: [10.13224/j.cnki.jasp.2012.12.015](https://doi.org/10.13224/j.cnki.jasp.2012.12.015).
11. ZHANG, H.J., GUO, R.W. and XIE, L.R. Design and validation of scheme over/under TBCC inlet, *J Aerospace Power*, November 2012, **27**, (11), pp 2475-2483. doi: [10.13224/j.cnki.jasp.2012.11.021](https://doi.org/10.13224/j.cnki.jasp.2012.11.021).

12. FAN, Y., CHANG, J., BAO, W. et al. Effects of boundary-layer bleeding on unstart oscillatory flow of hypersonic inlets. *Aeronautical J*, July 2010, **114**, (1157), pp 445-450. doi: [10.1017/S0001924000003924](https://doi.org/10.1017/S0001924000003924).
13. NAKAYAMA, T., SATO, T., AKATSUKA, M. et al. Investigation on shock oscillation phenomenon in a supersonic air inlet, AIAA Paper 2011-3094, 2011.
14. OGAWA, T., WATANABE, Y., MURAKAMI, A. et al. Shock wave oscillation phenomena depending on boundary layer conditions in transonic flow, AIAA Paper 2008-717, 2008.
15. ZHANG, H.J., LIU, X.G., GUO, R.W. and XIE, L.R. Design of turbo diffuser for TBCC inlet and characteristics of turbo mode, *J Aerospace Power*, January 2014, **29**, (1), pp 181-191. doi: [10.13224/j.cnki.jasp.2014.01.024](https://doi.org/10.13224/j.cnki.jasp.2014.01.024).
16. CHENG, D.S., TAN, H.J., SUN, S. and TONG, Y. Computational study of a high-performance submerged inlet with bleeding vortex, *J Aircraft*, March 2012, **49**, (3), pp 853-860. doi: [10.2514/1.C031483](https://doi.org/10.2514/1.C031483).
17. SPALART, P.R. and ALLMARAS, S.R. A one-equation turbulence model for aerodynamic flows, AIAA Paper 92-0439, 1992.
18. NEWSOME, R.W. Numerical simulation of near-critical and unsteady, subcritical inlet flow, *AIAA J*, October 1984, **22**, (10), pp 1375-1379. doi: [10.2514/3.48577](https://doi.org/10.2514/3.48577).
19. CHANG, J.T., WANG, L., BAO, W. and QIN, J. Novel oscillatory patterns of hypersonic inlet buzz, *J Propulsion and Power*, June 2012, **28**, (6), pp 1214-1221. doi: [10.2514/1.B34553](https://doi.org/10.2514/1.B34553).
20. TAN, H.J., LI, L.G., WEN, Y.F. and ZHANG, Q.F. Experimental investigation of the unstart process of a generic hypersonic inlet, *AIAA J*, February 2011, **49**, (2), pp 279-288. doi: [10.2514/1.J050200](https://doi.org/10.2514/1.J050200).
21. HYOUNG, J.L., BOK, J.L., SUNG, D.K. and JEUNG, I.S. Flow characteristics of small-sized supersonic inlets, *J Propulsion and Power*, February 2011, **27**, (2), pp 306-318. doi: [10.2514/1.46101](https://doi.org/10.2514/1.46101).
22. VIVEK, P. and MITTAL, S. Buzz instability in a mixed-compression air intake, *J Propulsion and Power*, March 2009, **25**, (3), pp 819-822. doi: [10.2514/1.39751](https://doi.org/10.2514/1.39751).